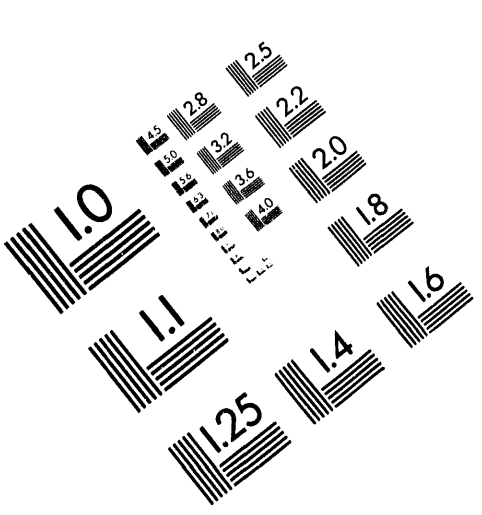

Association for Information and Image Management

1100 Wayne Avenue, Suite 1100
Silver Spring, Maryland 20910

301/587-8202

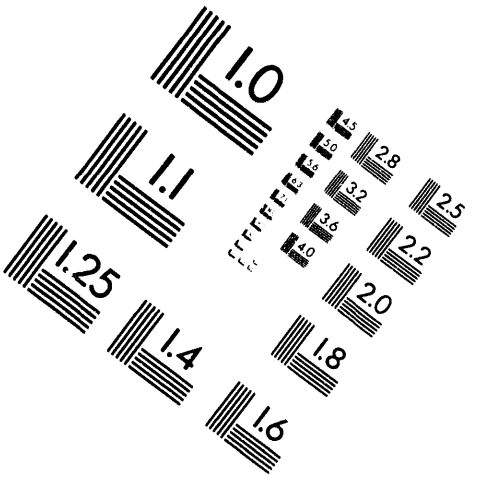

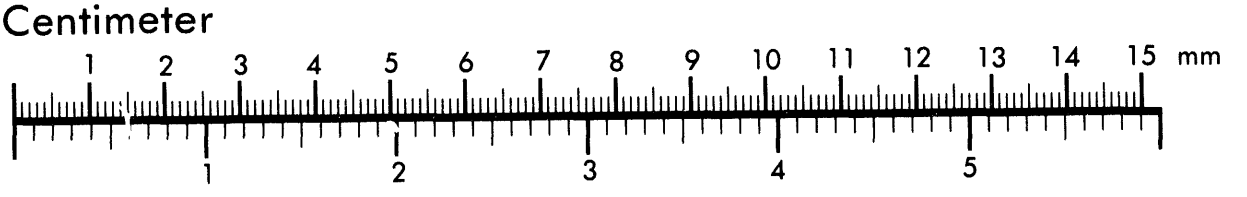

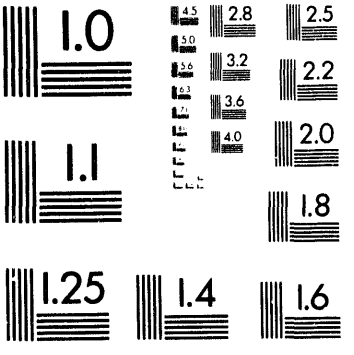

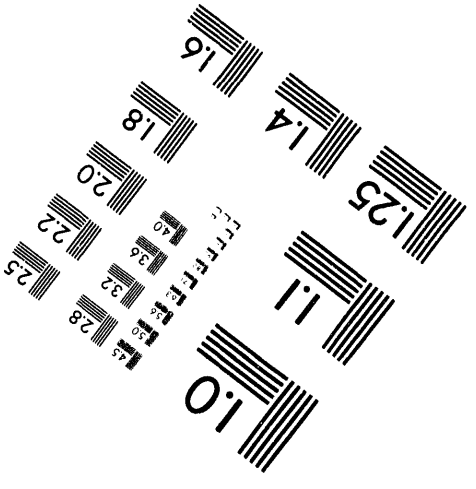

MANUFACTURED TO AIIM STANDARDS
BY APPLIED IMAGE, INC.

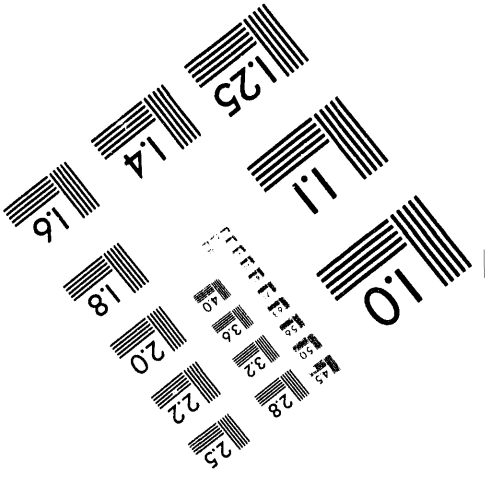

1 of 1

2

Conf-9410203--1

UCRL- JC- 117630
PREPRINT

The Influence of Chemistry and Microstructure on the Fracture Toughness of V-V_3Si In-Situ Composites

G. A. Henshall
M. J. Strum
B. P. Bewlay
J. A. Sutliff

This paper was prepared for submittal to:
Fatigue and Fracture of Ordered Intermetallic Materials II, Rosemont, IL, October 3-6, 1994

August 19, 1994

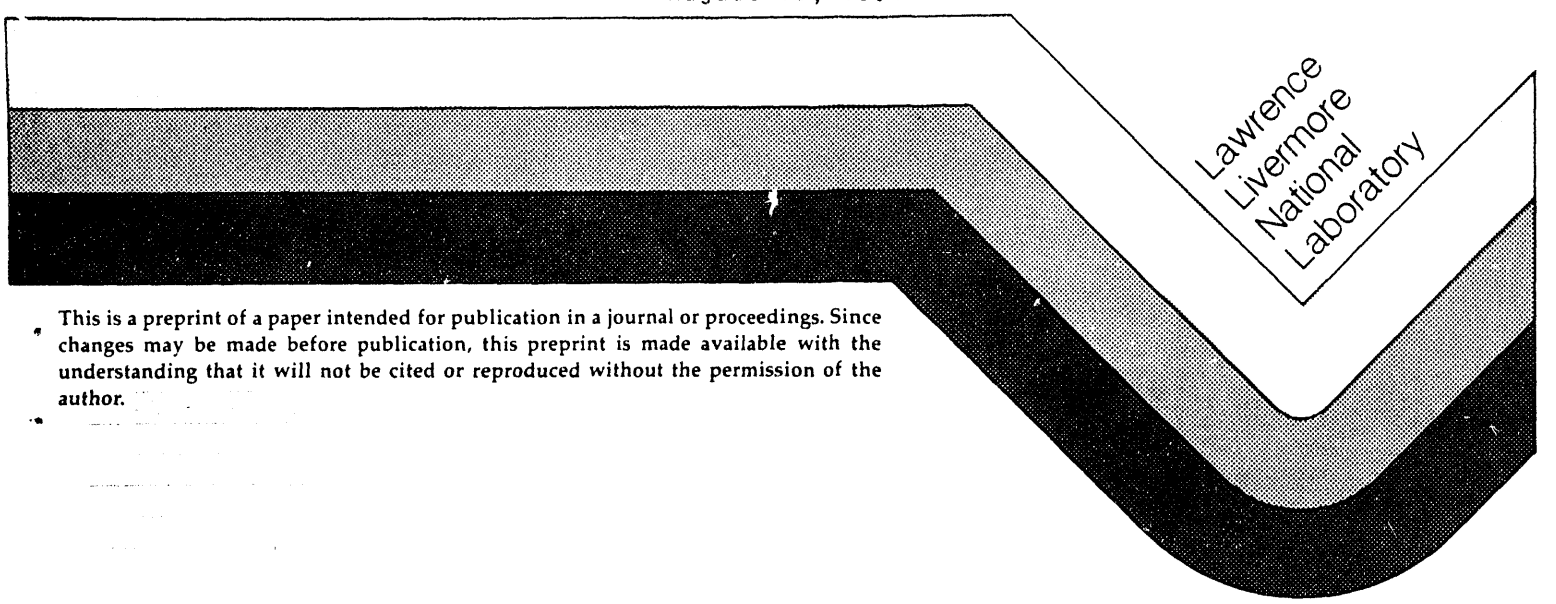

THE INFLUENCE OF CHEMISTRY AND MICROSTRUCTURE ON THE FRACTURE TOUGHNESS OF V-V_3Si IN-SITU COMPOSITES

G. A. Henshall[1], M. J. Strum[1], B. P. Bewlay[2], and J. A. Sutliff[2]

[1] Lawrence Livermore National Laboratory
P. O. Box 808
Livermore, CA 94551

[2] GE Corporate Research and Development Laboratory
P. O. Box 8
Schenectady, NY 12301

Abstract

The room temperature fracture behavior is described for ductile-phase toughened V-V_3Si *in-situ* composites produced by arc melting (AM), cold-crucible induction melting (IM), and cold-crucible directional solidification (DS). Composites were produced containing a wide range of microstructures, interstitial impurity contents, and volume fractions of the ductile V-Si solid solution phase, denoted (V). The fracture toughness of these composites generally increases as the volume fraction of (V) increases. For a given volume fraction of (V), the fracture toughness increases with decreasing "effective" interstitial impurity content, [I]=[N]+1.33[O]+9[H]. In eutectic composites, as [I] decreases from 1400 ppm (AM) to 400 ppm (IM), the fracture toughness increases from 10 to 20 MPa $\sqrt{m}$. The fracture toughness of the V-V_3Si composites is further correlated with the mechanical properties of the component phases, SEM observations of the fracture surface characteristics, and electron back-scattering pattern measurements of the fracture facet crystallography. These correlations are discussed with respect to conventional ductile phase "bridging" theories.

INTRODUCTION

Structural applications of many monolithic intermetallic compounds are limited by their low intrinsic fracture toughness. However, intermetallic ductile-phase toughened composites, which have been generated using both artificial [1-4] and *in-situ* [5-7] methods, can possess substantially higher fracture toughnesses. The *in-situ* approach, in which the ductile phase is dispersed by phase separation during solidification, is the focus of the present study because of its potential for relatively low cost production. In addition, the composites produced have good thermochemical stability compared with artificial composites.

Using V-V_3Si as a model system [8,9], composites were produced with a wide range of microstructures, interstitial impurity contents, and volume fractions of the ductile V-Si solid solution phase by adjusting the Si content and by selecting different casting methods. One advantage of the V-Si system over some other refractory metal systems for fundamental studies of *in-situ* ductile-phase toughening is the suitable phase equilibria. The more technologically important and well-studied Nb-Si system, for example, has a more complex phase diagram, resulting in more complex microstructures [7,10]. In contrast, the V-Si phase diagram [11] contains a simple eutectic between the intermetallic and the ductile metal phase, leading to simple composite microstructures. Specifically, a eutectic occurs at approximately 1870 °C and 7.6 wt.% Si (all compositions given in this paper are in weight percent). At the eutectic temperature the bcc V-Si solid solution, denoted (V), contains 4% Si and the V_3Si (A15 structure), which also exists as a solid solution, has a composition of 11% Si. These concentrations change as the temperature decreases from the eutectic, but below about 1400 °C the compositions of the two solid solutions remain nearly constant at 2.7% Si for the (V) and 13.1% Si for V_3Si.

In the present paper, the measured room temperature fracture toughness of the V-V_3Si composites is discussed in relation to current theories of ductile-phase toughening, for which crack bridging is the most prominent. Analysis of the toughness enhancement provided by ductile-phase bridging has been performed by several investigators [12-21]. These analyses assume constrained deformation of a single bridging particle much larger in size than the local crack opening displacement; the particle deforms and fails in a ductile manner behind the crack tip. The most common expression for small, steady-state bridging zones is that of Ashby *et al.* [12], in which the composite fracture toughness, K_c, is given by

$$K_c = K_m + E\left[C\,V_f\,\frac{\sigma_o}{E}a_o\right]^{1/2} \quad , \tag{1}$$

which depends on K_m, the fracture toughness of the matrix, and the modulus, E, volume fraction, V_f, yield strength, σ_o , and radius, a_o, of the ductile phase. The constraint parameter, C, which is proportional to the work required to rupture the ductile phase, is given by

$$C = \frac{1}{\sigma_o a_o}\int_0^{u^*}\sigma(u)\,du \ , \tag{2}$$

where σ is the nominal tensile stress in the ductile phase, u is the displacement of the ductile phase, and u^* is the displacement of the ductile phase at rupture. Depending on the extent of the interphase debonding and the material system, experimentally determined values of C typically vary between 1.6 and 6.0 [12]. The value of C, and hence the composite toughness, generally increase as the debond length increases [12-21]. One aim of the present study was to evaluate the extent of ductile bridging in V-V_3Si *in-situ* composites and the usefulness of eqn. (1) in describing the fracture toughness of composites with varying fractions of the ductile phase, *i.e.* $K_c \sim (V_f)^{1/2}$. Further, the effects of composite chemistry and microstructure on the fracture behavior have been examined.

EXPERIMENTAL MATERIALS AND PROCEDURES

The composites used in this study were prepared by arc melting, induction melting, and directional solidification. The first series of arc-melted alloys (AM-1) was cast using pieces of 99.8% pure V sheet that were acid cleaned in a HNO_3/HF solution. The second series of arc-melted alloys (AM-2), and all other alloys, were prepared using 99.9% pure V chips with low interstitial concentrations (120 ppm O, 80 ppm C, 26 ppm N, and < 3 ppm H). High-purity Si (99.999 %) was used for all castings. Directionally solidified (DS) and induction melted (IM) composites were produced using a segmented, water-cooled copper crucible with a partially levitated melt [22]. Directional solidification was achieved using a Czochralski method in which a DS seed crystal was lowered into the melt and withdrawn at 5 mm/min. to produce an aligned composite approximately 10 mm in diameter and 75 mm in length. The IM castings were prepared similarly to the DS castings except they were allowed to re-solidify within the crucible without being

withdrawn, resulting in a non-aligned microstructure. All of the alloys were triple melted in high-purity argon atmospheres to improve their homogeneity and to minimize interstitial contamination. The chemical compositions of the alloys, which are listed in Table I, were determined by spectrographic and LECO inert gas fusion methods. The interstitial contents were sensitive to both the V melting stock and the casting method. The cold crucible methods resulted in a significant decrease in the interstitial concentrations relative to arc melting.

Table I. Alloy chemical compositions.

Designation	Nominal vol. % (V)	Si (wt. %)	V (wt. %)	O (ppm)	N (ppm)	H (ppm)	[I] (ppm)
AM-2	100	2.7	97.2	290	370	30	1026
IM	100	2.84	97.1	250	43	19	546
AM-1†	90	4.21	95.7	470	810	9	1516
DS	90	5.24	94.7	210	40	5	364
AM-1	70	5.42	94.5	260	370	52	1184
AM-1†	50	7.66	92.2	410	870	4	1451
AM-2	50	7.3	92.6	260	280	72	1274
DS	50	7.3	92.6	130	58	22	429
IM	50	7.25	92.7	200	30	9	377
AM-1	30	10.0	89.9	240	480	20	979
DS	15	11.5	88.4	170	51	9	358

† Degassed for 1 h at 800 °C after arc melting.

Fracture toughness measurements were performed in three-point bending using single-edge-notched specimens with dimensions of approximately 3.5 x 7 x 30 mm. The specimens were tested at a span of 28 mm and a displacement rate of 0.02 mm/s. All specimens were fabricated and notched by electro-discharge machining with a notch opening width of 0.3 mm and a normalized crack length, a/w, of 0.45. Pre-cracking was performed under continuous loading and crack resistance data were measured by unloading immediately after each crack extension. Crack lengths were measured optically from metallographically polished specimen surfaces that were parallel to the crack propagation direction and perpendicular to the crack plane. Since ASTM standards

could not be rigorously met using these subsize specimens, the fracture toughness results are reported as K_Q instead of K_c.

Determination of the crystallographic fracture planes on the surface of failed bend specimens was performed in the SEM using a two-step process. First, the crystallographic orientations of grains on the fracture surfaces were determined using the electron back-scattering pattern (EBSP) technique for electron diffraction in the SEM [23]. Second, the corresponding facet normals were determined from a pair of tilting experiments, from which two vectors in the surface facet could be determined; the facet normal then was computed by a simple vector cross product. Conventional SEM and optical microscopy also were used to examine the fracture surface characteristics and the microstructures for each alloy.

EXPERIMENTAL RESULTS

Microstructures

The AM, IM, and DS casting methods and the different alloy compositions resulted in a range of microstructures. Beginning with the nominal eutectic alloys (7.25 - 7.66% Si), which consisted of nearly equal volume fractions of discontinuous V_3Si rods in a (V) matrix, Figs. 1 and 2 show the influence of casting method on the microstructure. In the AM and IM castings, the solidification structure was cellular, with cell diameters of 75 to 100 μm and lengths of 150 to 200 μm. The individual V_3Si rod orientations were related within a cell but varied from cell to cell. Rod aspect ratios of up to 20:1 were present in all of the eutectics. As shown in Fig. 2, the DS castings also possessed a cellular structure but the cells were highly elongated with diameters of 100 to 200 μm and lengths of at least 1.5 to 2 mm. Within the cell cores the V_3Si intermetallic rods exhibited strong alignment with the DS growth direction but the orientation varied within the intercellular boundaries. The rod diameters were larger in the DS castings than either the AM or IM castings. Typical rod diameters within the cell cores were between 1 and 1.5 μm in the AM and IM castings, and 1.5 to 3 μm in the DS castings. In all cases, the intercellular regions had a coarse eutectic structure with V_3Si rods up to 4 μm in diameter; the size of the (V) regions scaled with the increased V_3Si rod diameters. Within the intercellular regions, occasional V_3Si dendrites were also present. These accounted for less than 1% of the casting volume except for the AM-1 alloy (7.66% Si), which contained approximately 2%. The AM-1 microstructure shown in Fig. 1(a) represents the maximum amount of primary V_3Si observed in the nominal eutectics. These findings suggest an actual eutectic composition of about 7.25% Si (Table I) [22].

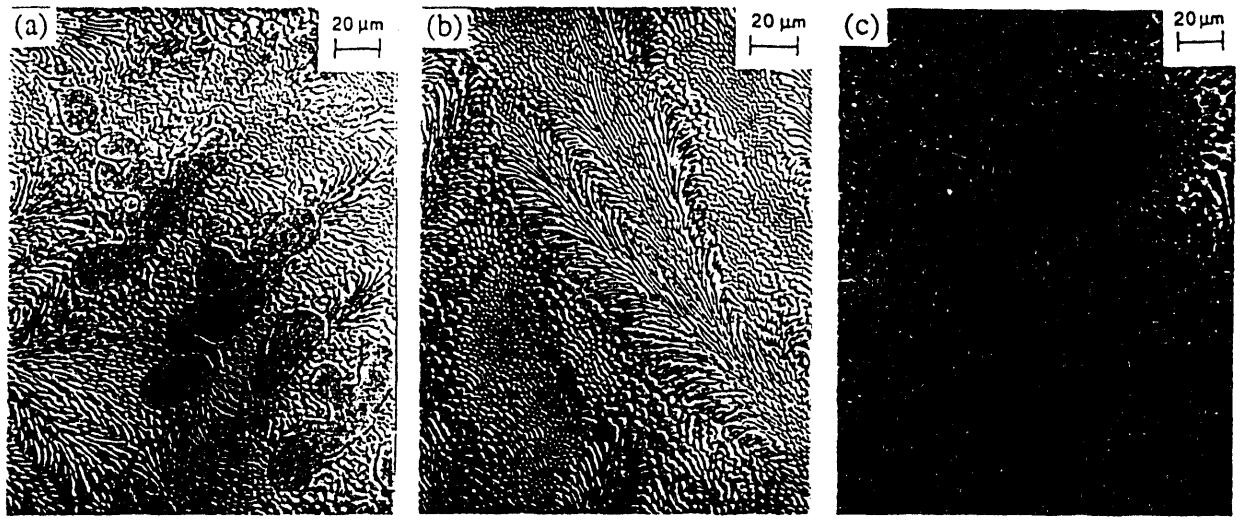

Figure 1. Typical microstructures for the nominal eutectic non-directional castings: (a) AM-1 (V-7.66% Si), (b) AM-2 (V-7.3% Si), and (c) IM (V-7.25% Si).

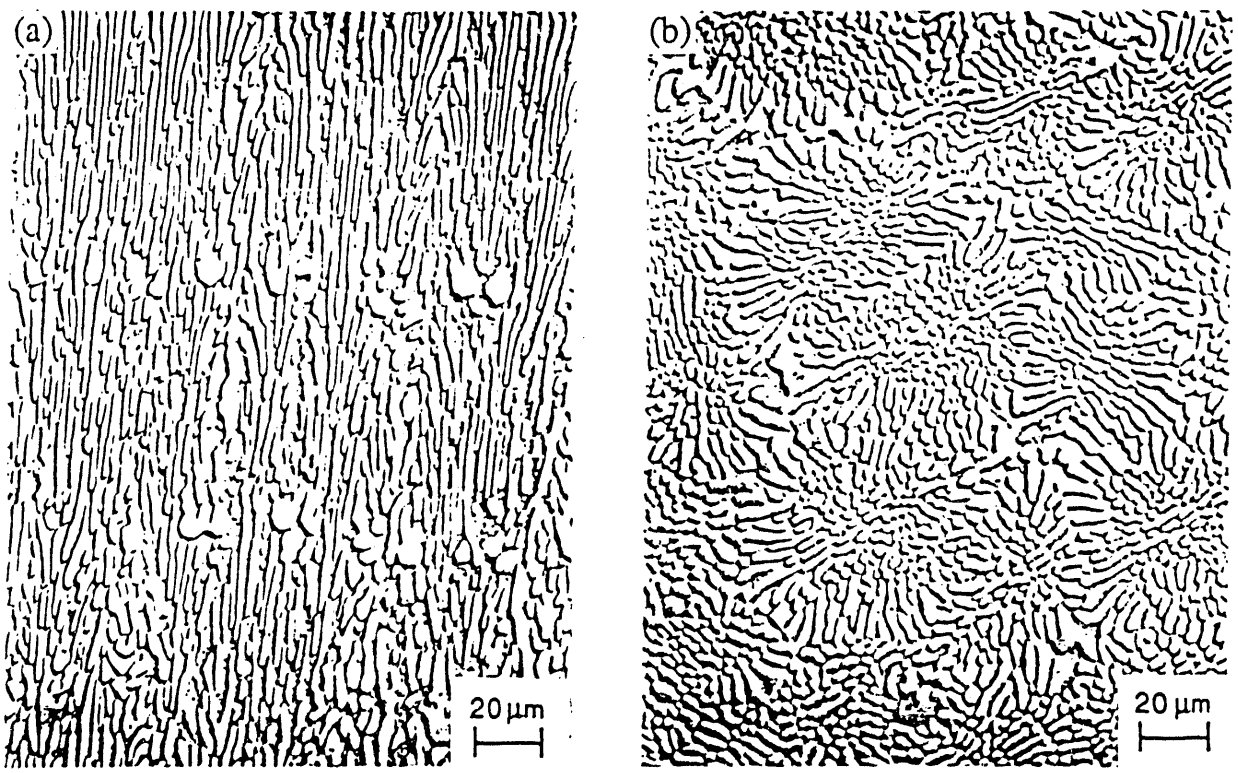

Figure 2. Typical microstructures for the directionally solidified eutectic casting (V-7.3% Si): (a) longitudinal direction and (b) transverse direction.

For off-eutectic compositions, the lowest Si content hypoeutectic alloys, with 2.7% (AM) and 2.8% (IM) Si, were essentially single phase and represent the composition of

the (V) phase. The V-4.2% Si alloy, Fig. 3(a), nearly matches the reported composition of maximum solubility of Si in V at the eutectic temperature [11]. This alloy contained approximately 10 volume pct. V_3Si, which was semi-continuous and was observed in the interdendritic regions. The nominal 70% (V) alloy, V-5.4% Si, consisted of primary (V) dendrites with an interdendritic eutectic of (V) and V_3Si, Fig. 3(b). As shown in Fig. 3(c), the hypereutectic nominal 30% ductile phase alloy, V-10% Si, contained a large fraction of V_3Si dendrites with interdendritic eutectic. A similar structure, but with a greater amount of V_3Si dendrites, was observed for the V-11.5% Si DS alloy. In all of the cast structures, including the hypereutectic alloys, the (V) was the continuous phase in the eutectic microconstituent.

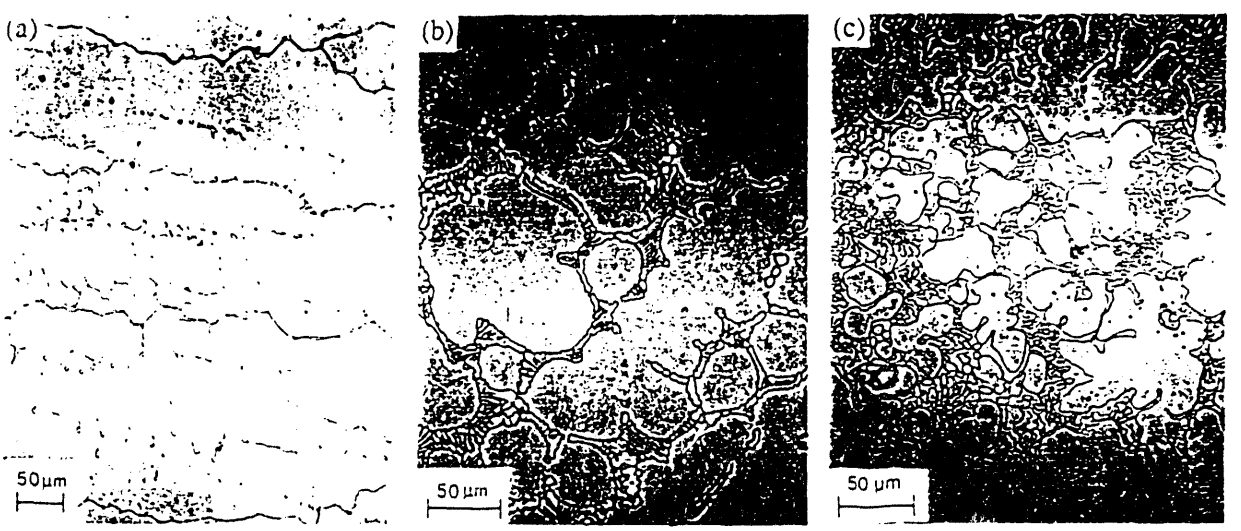

Figure 3. As-cast microstructures for the series-1 AM composites: (a) V-4.2% Si, (b) V-5.4% Si, and (c) V-10.0% Si.

Composite Fracture Behavior

The effect of the volume fraction of the ductile (V) phase, V_f, on the room temperature fracture toughness, K_Q, of V-V_3Si *in-situ* composites is shown in Fig. 4. The fracture toughness of V_3Si was estimated from the length of cracks emanating from the corners of pyramidal microhardness indentations to be 1.3 MPa$\sqrt{m}$ [8]. Clearly, the room temperature fracture toughness of V_3Si can be greatly increased by *in-situ* ductile-phase toughening with (V). With the exception of the anomalously low fracture toughness for the 90% (V) DS alloy, which will be discussed later, K_Q increases monotonically with

increasing V_f. (In contrast, Bewlay *et al.* [10] have shown that the fracture toughness of more microstructurally complex Nb-Si composites reaches a minimum at the eutectic composition and increases approximately linearly as the Si content either increases or decreases away from the eutectic composition.) Finally, the improvement in K_Q produced by the cleaner DS and IM casting methods over arc melting is shown in Fig. 4.

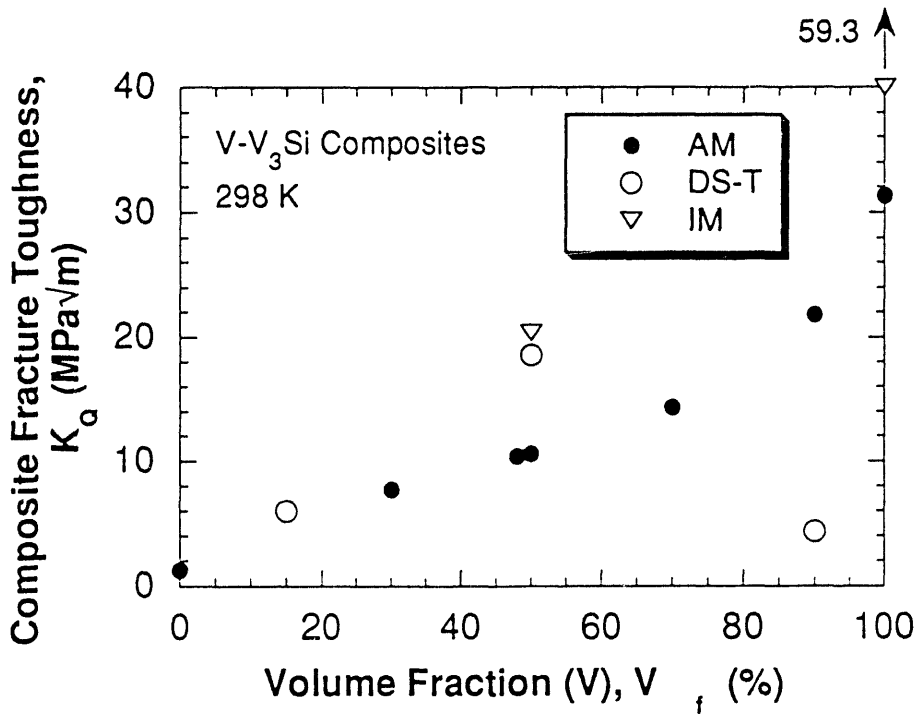

Figure 4. The room temperature fracture toughness as a function of the (V) volume fraction for arc-melted (AM), induction melted (IM), and directionally solidified (DS-T) *in-situ* V-V_3Si composites.

The fracture toughness of the eutectic alloys is plotted as a function of normalized crack length, *a/w*, in Fig. 5. The toughnesses of the AM-1 and AM-2 eutectic alloys were similar, with average values of 10.4 and 10.6 MPa$\sqrt{m}$. K_Q for the DS casting (tested such that the crack propagated transverse to the growth direction) was significantly higher, 18.5 MPa$\sqrt{m}$, and that of the IM alloy was the highest at 20.4 MPa$\sqrt{m}$. Figure 5 also shows the absence of any significant changes in toughness with crack propagation, or "R-curve" behavior. The data appear evenly scattered about the average K_Q, indicating the absence of significant bridging zone development with increasing crack length.

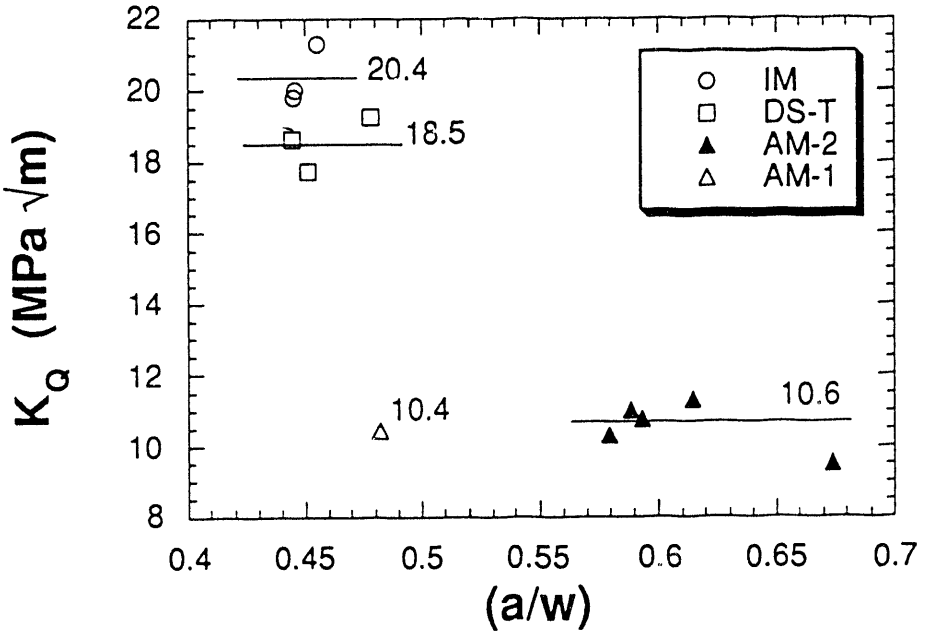

Figure 5. The fracture toughness of the nominal eutectic composites as a function of the normalized crack length, *a/w*.

As illustrated in Fig. 6, the fracture surfaces of the eutectic alloys produced by all methods contained mixtures of two types of zones: large cleavage zones and fine "micro-roughened" zones. The cleavage zones typically consisted of a large number of nearly parallel facets corresponding to individual V_3Si rods connected by smooth or stepped regions corresponding to the intervening (V) ligaments. There was little stretching of (V) in these regions, as shown in Fig. 7(a) for the AM-2 eutectic casting. Conversely, the micro-roughened zones consisted of V_3Si rods containing secondary cracks and (V) ligaments displaying considerable plastic extension, Fig. 7(b). Similar behavior was observed in the IM and DS alloys. The size and fraction of the macroscopic cleavage zones were largest for the AM alloys, and decreased for the DS and IM materials. It is estimated that cleavage zones accounted for 61% of the AM fracture surface area while only about 13% for the DS eutectic and 15% for the IM eutectic.

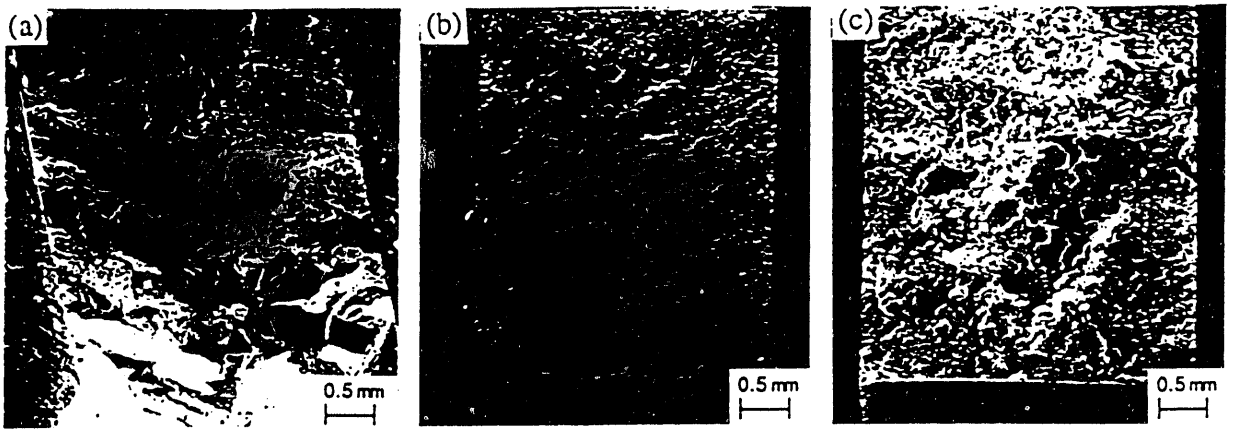

Figure 6. Fracture surfaces of (a) AM-2, (b) DS-T, and (c) IM eutectic composites.

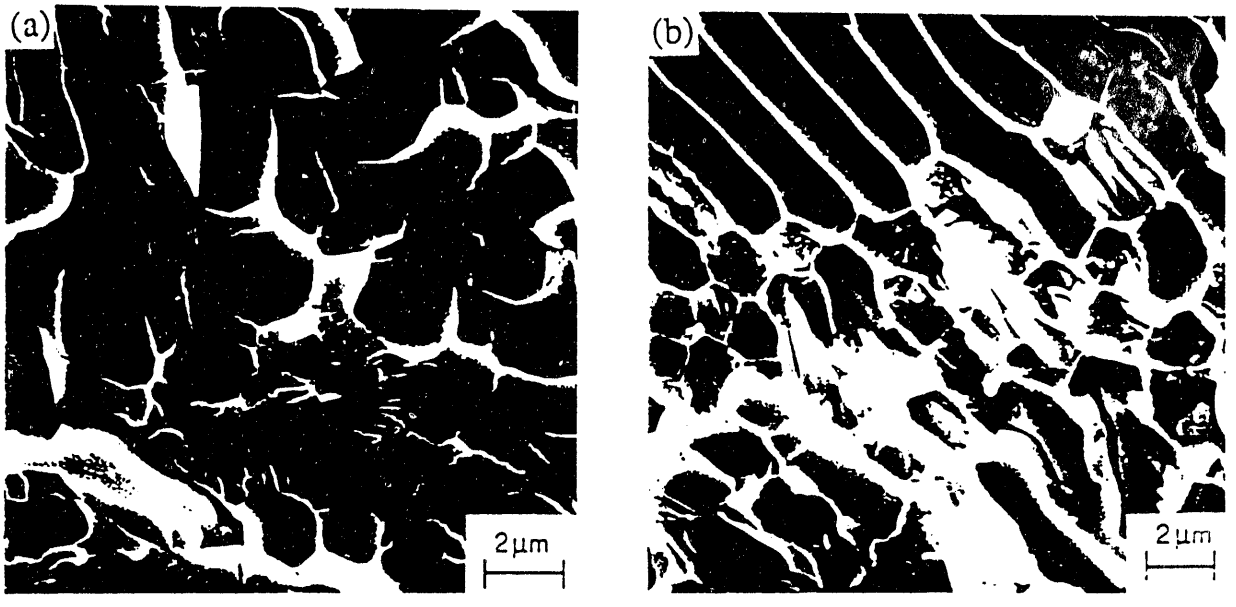

Figure 7. SEM fractographs of the AM-2 eutectic composite showing regions of (a) cleavage and (b) micro-roughening.

DISCUSSION

Effect of Ductile Phase Volume Fraction on Fracture Toughness

The influence of the (V) volume fraction, V_f, on the composite fracture toughness shown in Fig. 4 is quite different from the square root dependence predicted by eqn. (1). Clearly, factors other than those implicit in the derivation of eqn. (1) are controlling the fracture toughness in the V-V_3Si *in-situ* composites. First, for composites with either

small (*e.g.* 15%) or large (*e.g.* 90%) V_f, the underlying mechanism from which eqn. (1) was derived, namely bridging of a brittle crack by a series of ductile ligaments, is unrealistic. This is indicated by the microstructures for these composites, such as that shown in Fig. 3(a) for the 90% V_f composite. This composite consists of large (V) regions with small, semi-continuous regions of V_3Si. Such a microstructure is not consistent with that assumed in deriving eqn. (1) [1,12]. For these extreme V_f composites, the simplest alternative to eqn. (1) is to assume that the composite K_Q is controlled by a rule of mixtures. However, the relationship between K_Q and V_f is not linear. In particular, consider the hypoeutectic AM composites with $V_f > 50\%$ in Fig. 4 (the data are insufficient to make a similar assessment for the DS alloys or for $V_f < 50\%$). The experimental K_Q values lie well below a linear rule-of-mixtures prediction between K_Q for the 100% ductile phase alloy and K_Q for either the eutectic or for V_3Si. Again, examination of the microstructure in Fig. 3(a) for the 90% ductile phase composite suggests a reason why this approach is inappropriate. It appears that the localization of the low toughness V_3Si at (V) dendrite boundaries could provide pathways for easy fracture, thereby decreasing K_Q by an amount greater than that predicted by a rule of mixtures.

For (V) volume fractions near 50%, where the ductile bridging model may have relevance, the $(V_f)^{1/2}$ dependence of K_Q also does not exist. Examination of the data in Fig. 4 for $30\% \leq V_f \leq 70\%$ shows a linear relationship similar to that observed for hypoeutectic Nb-Si *in-situ* composites [10]. For these near-eutectic alloys, one possible reason for the deviation from the $(V_f)^{1/2}$ dependence predicted by eqn. (1) is that ductile-phase toughening mechanisms other than crack bridging may be contributing to K_Q. Possible mechanisms include [10,17] microcracking, crack deflection, and crack blunting. Evidence for the first two can be found in Figs. 6 and 7, and evidence for the latter stems from observations of cracks emanating from microhardness indentations that abruptly stop at (V) dendrites.

In addition to possible contributions from mechanisms other than bridging, the unexpected influence of V_f on K_Q for the near-eutectic composites may be affected by the fact that not all of the (V) in the composites contributes to ductile bridging. A similar observation was made by Bewlay *et al.* [10] for Nb-Si alloys. First, consider only the eutectic composites. As shown in Figs. 6 and 7, the eutectic (V) exhibits ductile stretching only within some regions of the fracture surface, while cleavage occurs in the others. Unfortunately, while K_Q decreased with increases in the total area fraction of cleavage, it is difficult to quantify the cleavage and bridging contributions. Crack propagation is governed by local conditions at the crack tip rather than an average

behavior across the entire fracture surface. To quantify the effects of cleavage, one would have to know what the fractions of cleavage and bridging fracture modes are along the length of the crack tip at each position for which K_Q vs. a/w data were taken. The corresponding measured K_Q values then could be correlated with these fractions. Such an undertaking was not attempted in this study.

In addition to regions within the eutectic composites for which the eutectic (V) is not ductile, neither was significant ductility observed in the (V) dendrites of the hypoeutectic alloys. Bewlay *et al.* [10] observed similar behavior in the (Nb) dendrites of hypoeutectic Nb-Si composites. They suggested that debonding may be less extensive in the dendrites than the high-aspect-ratio eutectic (Nb), leading to a larger degree of constraint and brittle behavior in the dendrites. The same may be true in the composites of the present study. In addition, IM and AM castings of bulk 100% (V), V-2.7% Si, fail in a brittle mode [8]. This result is somewhat surprising given the ductility of the (V) ligaments shown in Fig. 7(b). The fact that the micron-sized eutectic (V) ligaments can undergo substantial plastic stretching while the bulk (V) is brittle may be due to the short slip lengths in the eutectic microconstituent. Short slip lengths limit the intensity of internal stresses at the head of dislocation pile-ups that, if large enough, could lead to crack initiation [24-26]. The large slip lengths in the primary (V) dendrites then may be partly responsible for their lack of ductility. Naturally, the brittle nature of the primary (V) dendrites, whatever the cause, precludes their participation in ductile bridging behavior. In this case, the linear behavior shown in Fig. 4 for $30\% \leq V_f \leq 70\%$ suggests that a rule-of-mixtures law may be more appropriate than eqn. (1) in this regime.

Another complication that may affect the K_Q vs. V_f behavior of the V-Si composites is that the cleavage stress of the (V) phase is anisotropic. As shown in Fig. 8, many flat facets exist on the fracture surface of the AM 100% (V) alloy. Due to the random orientation of grains, many of these facets are highly inclined to one another. The crystallographic orientations of the grains on the fracture surface were determined using EBSP and the surface normal of each facet was determined by tilting in the SEM. As detailed elsewhere [27], the {001} poles of the bcc lattice correlate strongly with the facet normals. This suggests that the {001} planes in the (V) may be easy cleavage planes. This cleavage anisotropy may explain the anomalously low K_Q of the DS 90% (V) alloy shown in Fig. 4. If the DS process aligned the {001} planes such that they were perpendicular to the growth direction, and thus the maximum principal stress during crack growth, then fracture could occur at a much reduced applied stress intensity. EBSP analysis is in progress to test this hypothesis.

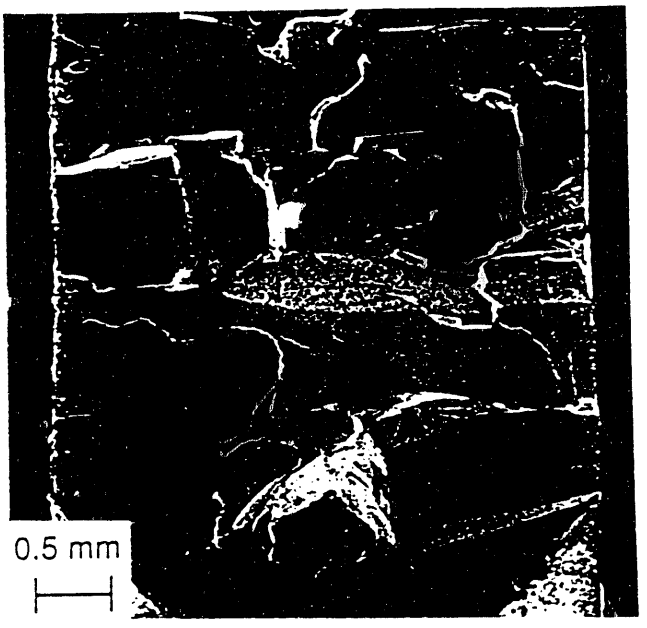

Figure 8. The fracture surface of the AM 100% (V) alloy (V-2.7% Si).

R-Curve Behavior

The lack of R-curve behavior for the eutectics, Fig. 5, is consistent with the moderate measured amount that the ductile (V) ligaments stretched in the micro-roughened regions and the correspondingly small steady-state bridging zone length. Both optical profiles [9] and atomic force microscopy (AFM) measurements suggest that the (V) ligaments stretched to modest lengths of approximately 0.25 to 0.3 times their diameter. As stated in the Introduction, theories suggest that the toughness increment provided by ductile-phase bridging increases rapidly as the debond length, and thus the amount of plastic stretching, approaches the diameter of the ductile ligament [12,13]. Further, following Bao and Hui [28] and Heredia *et al.* [17], the steady-state bridging zone length, L_{ss}, is given approximately by

$$L_{ss} = \frac{0.12\,\pi u^* E_c}{\sigma^*}\,, \tag{3}$$

where E_c is the composite Young's modulus, σ^* is the peak nominal tensile stress achieved in the ductile particles during fracture, and u^* is the ductile ligament failure displacement. For a debond length, h, equal to the ductile ligament radius a_o, $u^* \approx h = a_o$ and $\sigma^* \approx \sigma_o$ [17]. For the V-V_3Si eutectics this gives $u^* = 1.5$ μm and $\sigma^* = 431$ MPa [8]. Using a simple rule of mixtures for the eutectics gives $E_c = 171.5$ GPa [8]. Thus, eqn. (3) predicts for the case of $h = a_o$ that $L_{ss} = 225$ μm. However, the observed

ligament lengths suggest that $u^* \approx h \approx 1/3\ a_o$. In this case, the ductile ligaments are more highly constrained and σ^* is significantly larger than σ_o, say approximately $4\sigma_o$ [17]. Substituting these values into eqn. (3) gives L_{ss} = 19 μm. Such a small steady-state bridging zone is consistent with the lack of measured R-curve behavior in Fig. 5.

Effect of Interstitials

The detrimental effect of interstitial elements on the fracture toughness of bcc refractory metals is well known. However, the interstitial impurity content is seldom considered in studies of refractory metal intermetallic composites. In the present study, however, the detrimental effect of interstitials on the fracture of V-V_3Si composites was specifically investigated. This analysis is based on the experimental data of Loomis and Carlson [29] showing that the room temperature Charpy impact toughness of pure V varies for concentrations of N, O, and H in the ratio of 1 to 1.33 to 9. Assuming that these ratios are similar for (V), the "effective" interstitial concentration, [I] = [N] + 1.33[O] + 9[H], was calculated for each casting and is given in Table I. The suggestion that [I] describes the fracture toughness behavior of (V) is supported by the data for the AM and IM 100% (V) alloys. The ratio of $(K_Q)^{IM}$:$(K_Q)^{AM}$ is nearly the same as the ratio of the corresponding [I] values. Therefore, K_Q for each eutectic composite is plotted as a function of [I] in Fig. 9. A linear fit, for reference, reveals a good correlation for all of the tests reported (which were performed with the crack propagating through a randomly oriented microstructure, AM and IM, or transverse to the growth direction, DS-T). Further increases in purity would be expected to improve toughness, but the data are insufficient to predict a linear or exponential increase. The influence of interstitial impurities on K_Q is further emphasized by the fact that the IM and AM eutectics have the most similar microstructures but K_Q for the IM alloy is nearly double that of the AM alloys. Instead, K_Q for the IM alloy is essentially the same as that of the DS-T specimen, which has an interstitial content similar to the IM alloy but a significantly different microstructure. Therefore, K_Q is more sensitive to the interstitial content than to the microstructure of the composite.

CONCLUSIONS

An investigation of the room temperature fracture behavior of V-V_3Si *in-situ* composites has led to the following conclusions.

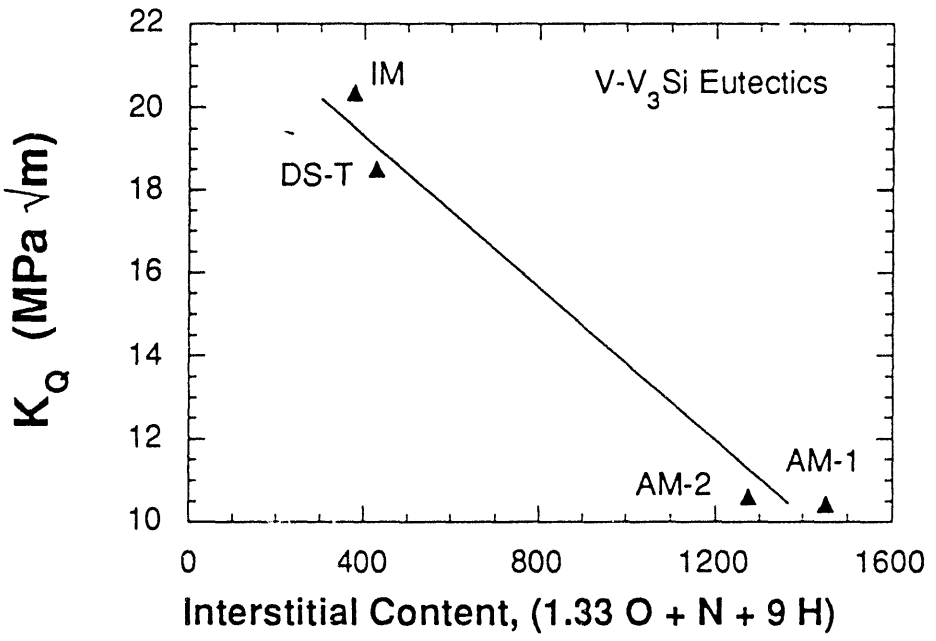

Figure 9. The fracture toughness of the eutectic composites as a function of the effective interstitial concentration.

1) The fracture toughness of V_3Si (~ 1.3 MPa $\sqrt{m}$) can be significantly improved by *in-situ* ductile-phase toughening with V. The fracture toughness of V-V_3Si composites is controlled by their microstructure and interstitial impurity content which, in turn, can be controlled by the casting method. For eutectic composites, which contain nearly equal volume fractions of the ductile phase and intermetallic V_3Si rods, a fracture toughness of over 20 MPa$\sqrt{m}$ was achieved.

2) For eutectic composites with a random or transverse orientation of the V_3Si rods with respect to the direction of crack propagation, the fracture toughness increases with decreasing "effective" interstitial concentration, [I] = [N] + 1.33[O] + 9[H]. The fracture toughness is predicted to increase above 20 MPa$\sqrt{m}$ for [I] < 300 ppm.

3) The fracture toughness of V-V_3Si *in-situ* composites increases monotonically with increases in the volume fraction of the ductile V-Si solid solution phase, (V). The square root dependence of fracture toughness on the volume fraction of the ductile phase predicted by theories of small-scale crack bridging is not observed in these composites. Several factors contribute to this result, including the lack of a microstructure capable of supporting classical bridging phenomena for large and small volume fractions of (V), and

the complex mechanical behavior of (V) depending on its purity, size, and orientation with respect to the applied principal stress.

4) The {001} planes in the (V) phase appear to be ones of easy cleavage. Since (V) is the continuous phase in the eutectic microconstituent, the cleavage anisotropy in this phase likely has a significant influence on the fracture mode of the composites.

ACKNOWLEDGMENTS

The authors would like to thank D. Hiromoto and R. Kershaw of LLNL for their contributions to the experiments. AFM measurements by Dr. M. Balooch of LLNL are gratefully acknowledged. Work by two of the authors (GAH and MJS) was performed under the auspices of the U. S. Department of Energy under contract no. W-7405-ENG-48 at the Lawrence Livermore National Laboratory.

REFERENCES

1. L. S. Sigl, *et al.*, "On the Toughness of Brittle Materials Reinforced with a Ductile Phase," *Acta Metall.* **39** (1988), 945-953.

2. H. E. Deve, *et al.*, "Ductile Reinforcement Toughening of γ-TiAl: Effects of Debonding and Ductility," *Acta Metall. Mater.* **38** (1990), 1491-1502.

3. L. Xiao and R. Abbaschian, "Role of Matrix/Reinforcement Interfaces in the Fracture Toughness of Brittle Materials Toughened by Ductile Reinforcements," *Metall. Trans.* **23A** (1992), 2863-2872.

4. W. O. Soboyejo, *et al.*, "Strength, Fracture, and Fatigue Behavior of Advanced High-Temperature Intermetallics Reinforced with Ductile Phases," *Metall. Trans.* **24A** (1993), 585-600.

5. J. J. Lewandowski, *et al.*, "Microstructural Effects on Ductile Phase Toughening of Nb-Nb Silicide Composites," in *High Temperature/ High Performance Composites*, F. D. Lemkey, *et al.*, eds., Mater. Res. Soc. Symp. Proc. **120** (1988), 103-109.

6. D. L. Anton and D. M. Shah, "Ductile Phase Toughening of Brittle Intermetallics," in *Intermetallic Matrix Composites*, D. L. Anton, *et al.*, eds., Mater. Res. Soc. Symp. Proc. **194** (1988), 45-52.

7. M. G. Mendiratta, J. J. Lewandowski and D. M. Dimiduk, "Strength and Ductile-Phase Toughening in the Two-Phase Nb / Nb_5Si_3 Alloys," *Metall. Trans.* **22A** (1991), 1573-1583.

8. M. J. Strum and G. A. Henshall, "Fracture Behavior of Vanadium/Vanadium Silicide In-Situ Composites," in *High-Temperature Ordered Intermetallic Alloys V*, I. Baker, *et al.*, eds., Mater. Res. Soc. Symp. Proc. **288** (1993), 1093-1098.

9. M. J. Strum, *et al.*, "The Effects of In-Situ Processing Methods on the Microstructure and Fracture Toughness of V-V_3Si Composites," in *High Temperature Silicides and Refractory Alloys*, C. L. Briant, *et al.*, eds., Mater. Res. Soc. Symp. Proc. **322** (1994), 511-516.

10. B. P. Bewlay, *et al.*, "Toughening Mechanisms in Directionally Solidified Nb-Nb_3Si-Nb_5Si_3 In-Situ Composites," in *Processing and Fabrication of Advanced Materials III*, V. Ravi, T. S. Srivatsan, and J. J. Moore, eds., TMS, Warrendale, PA (1994), 547-565.

11. J. F. Smith, *Phase Diagrams of Binary Vanadium Alloys* (Metals Park, OH: ASM International, 1989), 261-267.

12. M. F. Ashby, F. J. Blunt and M. Bannister, "Flow Characteristics of Highly Constrained Metal Wires," *Acta Metall.* **37** (1989), 1847-1857.

13. H. E. Deve and M. J. Maloney, "On the Toughening of Intermetallics with Ductile Fibers: Role of Interfaces," *Acta Metall. Mater.* **39** (1991), 2275-2284.

14. M. Bannister and M. F. Ashby, "The Deformation and Fracture of Constrained Metal Sheets," *Acta Metall. Mater.* **39** (1991), 2575-2582.

15. M. Bannister, *et al.*, "Toughening in Brittle Systems by Ductile Bridging Ligaments," *Acta Metall. Mater.* **40** (1992), 1531-1537.

16. L. Xiao and R. Abbaschian, "On the Flow Behavior of Constrained Ductile Phases," *Metall. Trans.* **24A** (1993), 403-415.

17. F. E. Heredia, *et al.*, "The Fracture Resistance of Directionallv Solidified Dual-Phase NiAl Reinforced with Refractory Metals," *Acta Metall. Mater.* **41** (1993), 505-511.

18. B. Budiansky, J. C. Amazigo and A. G. Evans, "Small-Scale Crack Bridging and the Fracture Toughness of Particulate-Reinforced Ceramics," *J. Mech. Phys. Solids* **36** (1988), 167-187.

19. K. S. Ravichandran, "A Survey of Toughness in Ductile Phase Composites," *Scripta Metall. Mater.* **26** (1992), 1389-1393.

20. K. S. Ravichandran, "The Mechanics of Toughness Development in Ductile Phase Reinforced Brittle Matrix Composites," *Acta Metall. Mater.* **40** (1992), 1009-1022.

21. P. A. Mataga, "Deformation of Crack-Bridging Ductile Reinforcements in Toughened Brittle Materials," *Acta Metall.* **37** (1989), 3349-3359.

22. K-M. Chang, *et al.*, "Cold-Crucible Directional Solidification of Refractory Metal Silicides," *J. of Metals* **44** (1992), 59-63.

23. V. Randle, *Microtexture Determination and its Applications* (London, Institute of Metals, 1992).

24. A. N. Stroh, "A Theory of Fracture of Metals," *Advan. Phys.* **6** (1957), 418-465.

25. A. H. Cottrell, "Theory of Brittle Fracture in Steel and Similar Metals," *Trans. AIME* **212** (1958), 192-203.

26. G. E. Dieter, *Mechanical Metallurgy, Second Edition* (New York, NY: McGraw-Hill, 1976), 262-271.

27. J. A. Sutliff, *et al.*, "Facet Crystallography of Fractured V(2.7 wt.% Si) Solid Solution" (Paper presented at the Microscopy Society of America Annual Meeting, New Orleans, August 1994).

28. G. Bao and C.-Y. Hui, "Effects of Interface Debonding on the Toughness of Ductile-Particle Reinforced Ceramics," *Int. J. Solids Structures* **26** (1990), 631-642.

29. B. A. Loomis and O. N. Carlson, "Investigation of the Brittle-Ductile Transition in Vanadium," in *Reactive Metals*, W. R. Clough, ed., Interscience Pub., New York (1958) 227-243.

DATE FILMED

10/31/94

END